MEMS-Based Diagnostics

For Turbulent Shear Flows

Final Technical Report

Grant Number: F49620-93-1-0495

Prepared By:

Prof. Ari Glezer, Mechanical Engineering
Prof. Mark Allen, Electrical and Computer Engineering
Prof. Martin Brooke, Electrical and Computer Engineering

Georgia Institute of Technology
Atlanta, GA 30332

Submitted To:

Drs. James M. McMichael / Mark Glauser
Air Force Office of Scientific Research
Bolling AFB, DC

REPORT DOCUMENTATION PAGE

AFOSR-TR-97

0255

1. AGENCY USE ONLY (Leave blank)	2. REPORT DATE	3. REPORT TYPE AND DATES COVERED
	04/16/97	Final Technical Report 08/15/93 - 02/14/97

4. TITLE AND SUBTITLE
MEMS-BASED DIAGNOSTICS FOR TURBULENT SHEAR FLOWS

5. FUNDING NUMBERS
F49620-93-1-0495

6. AUTHOR(S)
Prof. Ari Glezer
Prof. Mark Allen
Prof. Martin Brooke

7. PERFORMING ORGANIZATION NAME(S) AND ADDRESS(ES)
Georgia Institute of Technology
Atlanta, GA 30332

8. PERFORMING ORGANIZATION REPORT NUMBER

9. SPONSORING/MONITORING AGENCY NAME(S) AND ADDRESS(ES)
AFOSR/NA
110 Duncan Avenue, Suite B 115
Bolling AFB, DC 20332-8050

10. SPONSORING/MONITORING AGENCY REPORT NUMBER

11. SUPPLEMENTARY NOTES

12a. DISTRIBUTION AVAILABILITY STATEMENT
Approved for public release; distribution unlimited.

12b. DISTRIBUTION CODE

13. ABSTRACT (Maximum 200 words)

The objective of this section of the research is to develop harware for fast processng of change-coupled display (CCD) images. This hardware will take digital CCD output and process it at the same output data rate of the CCD. The result is processed images at the maximum rate possible with a CCD camera. In particular, the hardware will perform convolutions of the input images with a digitally stored convolution kernal matrix, such as are needed for image spatial filtering and neutral networks.

A hardware test chip has been completed, characterized, and has been used to process images. This chip does not contain the digital front end necessary to connect directly to a CCD data stream but does demonstrate all of the critical analog components of the image processor. The test chip will be integrated with a shift register in a later chip fabrication to produce a fully functional image processor chip capable of connection to the data stream directly output from a CCD or similar row-wise serial output imaging device.

14. SUBJECT TERMS

15. NUMBER OF PAGES

16. PRICE CODE

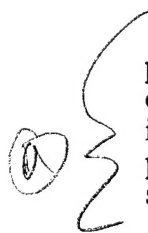| 17. SECURITY CLASSIFICATION OF REPORT	18. SECURITY CLASSIFICATION OF THIS PAGE	19. SECURITY CLASSIFICATION OF ABSTRACT	20. LIMITATION OF ABSTRACT
Unclassified	Unclassified	Unclassified	

1. AASERT Student Progress

There are two students who have been supported on this AASERT grant. Mr. Brent Buchanan is under the direction of Prof. Martin Brooke, and Mr. David Coe is under the direction of Prof. Mark Allen. Both students are making satisfactory progress toward completion of their Ph.D. degrees, as assessed both by their respective advisors as well as the School of Electrical and Computer Engineering. It is anticipated that both students will finish their degrees in 1997 (this year).

Mr. Buchanan has primarily been responsible for development of neural network architectures for deconvoluting flow information from flow sensors which have either been embedded into the flow or which have used optical means to sense flow information. Mr. Coe has been responsible for the development of a new class of actuators, the micromachined jet or *microjet*, which is a micromachined synthetic jet capable of momentum injection (but no mass injection) into the flow.

Only summaries of the work are given in the report. Full details are given in the previous progress reports as well as scientific papers in the references, most of which have been previously submitted to AFOSR.
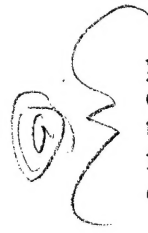
2. Analog neural net hardware for diagnostic processing

2.1 Objectives

The objective of this section of the research is to develop hardware for fast processing of charge-coupled display (CCD) images. This hardware will take digital CCD output and process it at the same output data rate of the CCD. The result is processed images at the maximum rate possible with a CCD camera. In particular, the hardware will perform convolutions of the input images with a digitally stored convolution kernal matrix, such as are needed for image spatial filtering and neural networks.

2.2 Status of Effort

A hardware test chip has been completed, characterized, and has been used to process images. This chip does not contain the digital front end necessary to connect directly to a CCD data stream but does demonstrate all of the critical analog components of the image processor. The test chip will be integrated with a shift register in a later chip fabrication to produce a fully functional image processor chip capable of connection to the data stream directly output from a CCD or similar row-wise serial output imaging device.

2.3 Accomplishments

2.3.1 Spatially Oversampled Filtering Theory

Since physical impracticalities prevent the straight-forward and compact design of high-order bit A/D converters in standard digital fabrication processes, it is desirable to develop an architectural design philosophy that can incorporate the low level of component precision that is readily available while concurrently achieving a suitably high system performance. A successful methodology that is now commonly used with the sampling of

audio signals, Delta-Sigma Quantization, involves signal oversampling and quantization noise shaping to produce a signal represented by small bit lengths, though at the expense of greater temporal granularization. This technique is readily extended to multi-dimensional signals such as images.

Intuitively, this procedure works by increasing the operational spectrum beyond the Nyquist demands of the signal and forcing the quantization noise energy into the unused portions of the widened spectrum. As the noise energy in the signal band is displaced, the in-band signal-to-noise ratio (SNR) increases though the total SNR remains the same (or, as in actual practice, slightly deteriorates) for a given level of quantization. This permits the signal to be represented with shorter bit-length samples, though more of them, and without compromising the information content of the signal. As long as the noise energy is not aliased into the signal band during subsequent processing steps, it may be harmlessly transported through the overall system or filtered off if necessary.

2.3.2 Image Processing Hardware Test Chip

A hardware test chip has been completed. The chip contains the analog-digital mixed signal portion of the proposed CCD image processing circuit. Specifically, this chip contains 512 A/D converters arranged in a 16x16 array of Multiplying A/D Converters (MDACs). Each of the 256 MDACs consists of two 5-bit A/D converters, two 5-bit digital storage registers, and a sign register. After the appropriate weight from the convolution kernel and pixel data from the image have been stored in the two storage registers, the multiplication is performed through the biasing of the data A/D Converter with the output of the weight A/D Converter. The sign register stores a bit which determines to which of two universally common nodes the output current is then tied. With one node corresponding to positive weights and the other negative weights, the difference in the output of these currents from the entire array of MDACs is then the result of the current convolution point. This chip has been tested for its ability to perform image processing tasks such as spatial filtering.

After characterizing the entire array of MDACs for performance and matching, a low-pass characteristic convolution kernel (a 16x16 "Mexican hat") was programmed into the weight registers and an image (Figure 2a) was passed through the chip with the use of an automated test bed. The test bed consisted of a PC with a digital output card running under LabView, and two SMUs under observation by a GPIB controller installed in the same PC. For purposes of comparison, an `ideal' resultant image was computed with a compiled using a compiled C program specially written for the purpose (Figure 2b). The image observed by the automated test bed appears in Figure 2c. Note that the circuit successfully removed the high frequency components of the original image while passing the low frequency portions of the image, but introduced a degree of high frequency (presumably broad spectrum) noise likely due to quantization effects.
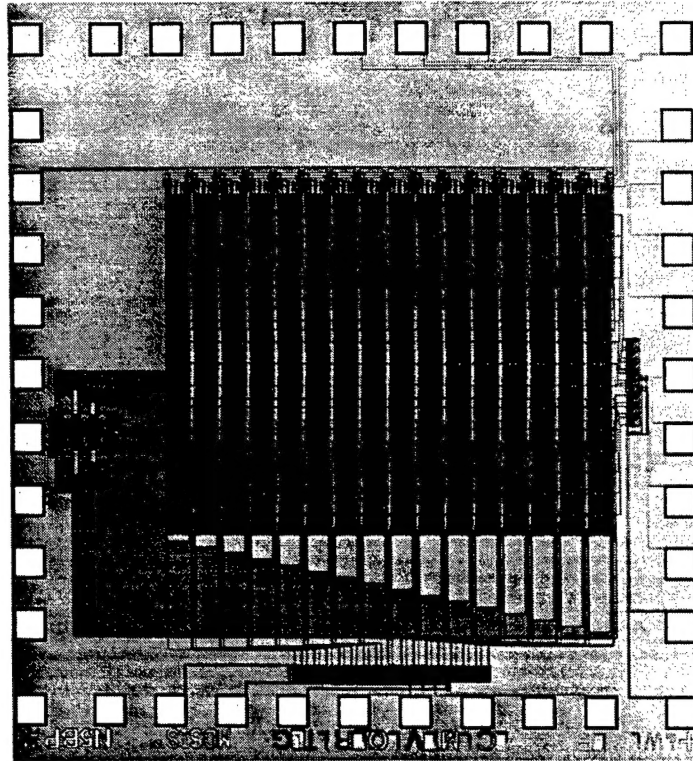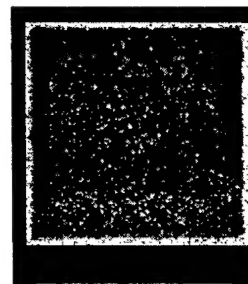
Figure 1: Analog Convolution Chip

(a)　　　　　　　(b)　　　　　　　(c)

Figure 2. *Chip input and output images. (a) 128x128 input image; (b) 113x113 computer generated floating-point output image; (c) 113x113 chip-generated mixed-signal output image*

3. Microjet Hardware for Flow Manipulation

3.1 Objectives

The objective of this phase of the effort is to develop microjet-based actuators which have the capability of affecting and manipulating flows. Ultimately it is hoped that these actuators can be coupled with appropriate (e.g., analog-hardware-based) sensing and control schemes such as those described above to create a complete flow manipulation system.

3.2 Status of Effort

Under this AASERT contract, synthetic jet technology which was developed under the parent grant has been implemented using standard (traditional) MEMS technology. A cross-section of a prototype micromachined version of the synthetic jet which has been developed at Georgia Tech [4,6] is shown in Figure 3. The polyimide film acts as a flexible diaphragm, the vibration of which causes jet emission from the orifice hole. Both integrated electrostatic excitation of the diaphragm (by applying a sinusoidal voltage between the two aluminum electrodes) as well as external drive of the diaphragm (e.g., by using a piezoelectric driving element) have been successfully used to realize microjets. A smoke visualization of the micromachined jet (rotated 90 degrees) is shown in Figure 4. The field of view measures 89 mm in the streamwise (x) direction and thus corresponds to nearly 500 jet diameters. The jet appears to become turbulent at or near the orifice, and spreads almost linearly with streamwise distance. Large coherent vortical structures are apparent in the far field of the jet. The Reynolds number of the jet based on the centerline velocity and its width at $x/D = 15$ (see velocity profiles in Figure 5) is approximately 1400.

The streamwise velocity component was measured using a miniature total pressure tube having inner and outer diameters of 212 μm and 340 μm, respectively. Radial profiles of the time-averaged streamwise velocity were measured at $x/D = 15$, 25, and 35 using a three-axis traversing mechanism. peak jet velocities of 15-20 m/s were achieved 15 diameters downstream of the orifice hole. The jet is reasonably symmetric about its centerline, and when jet velocity profiles are plotted in similarity coordinates they collapse reasonably well on top of each other, suggesting that the jet is self-similar.

This work has also been extended to micromachined jet arrays which are individually addressable [4]. The addressable microjet array consists of an array of small orifices situated on top of an array of actuator cavities. Both the orifices and the cavities are batch fabricated from (100) silicon using micromachining techniques. The length of an orifice is defined by the wafer thickness, typically 250 μm, while the depth of the actuator cavity is approximately 15 microns. Typical orifice lateral dimensions range from 50-800 μm. Individual jet control is achieved by use of a metallized flexible polyimide diaphragm, or by use of electrothermally driven modulators at each orifice. The metal electrodes on the diaphragm are patterned so that voltage can be individually applied to the region over each actuator cavity. Similarly to the individual microjets, the diaphragm can be vibrated using either a commercial piezoelectric transducer to drive all array elements in parallel or a sinusoidal drive voltage applied to the flexible diaphragm of individual array elements. Driving the membrane in either fashion results in cavity pressure variations and a jet flow through the orifice. An individual jet is modulated by either reducing the amplitude of the drive voltage of an individual array element (for electrostatic drive) or by electrostatically modulating the diaphragm vibration amplitude for that element (for piezoelectric drive).
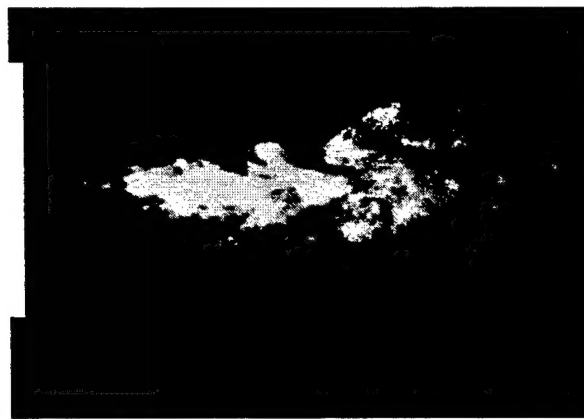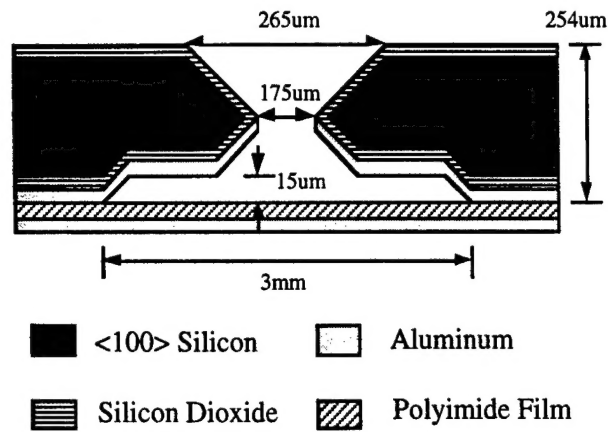
Figure 3. *Left: Schematic of micromachined synthetic jet; Right: Smoke visualization of operational jet.*

The above hardware demonstrates that it is feasible to use MEMS technology to microfabricate arrays of individually addressable synthetic jets. Recently, new drive elements based on electromagnetic drive have been investigated to reduce unwanted noise emitted by the jet generation actuators. In addition, a scheme to produce more robust microjets with an eye towards eventually being able to manipulate flows of practical aerodynamic interest has been investigated and is currently under development. This scheme involves the use of conventional drivers to generate higher-momentum microjet arrays, and highly interconnected and batch fabricated modulators at the output of each orifice hole of the array to control and modulate the robust jet output. Successful modulation of jets in excess of 20 m/s using batch-fabricated, MEMS-based modulators has been achieved.

In the robust designs, the microjet array consists of a silicon wafer with an array of anisotropically-etched orifices through the wafer. A bimetallic beam is suspended above each orifice to serve as the valve flap. Attached to the back of the wafer is an external membrane driven continuously by either a piezoelectric or electromagnetic driving element. When an electrical current is passed through a particular bimetallic beam structure, the resulting heat causes the beam structure to bend (either vertically or horizontally, depending upon the design) uncovering an orifice to allow a synthetic jet to flow through it. The advantage of this microjet design is that it decouples the jet generation and jet modulation functions, thereby reducing the demands on the microactuator elements and simplifying fabrication.
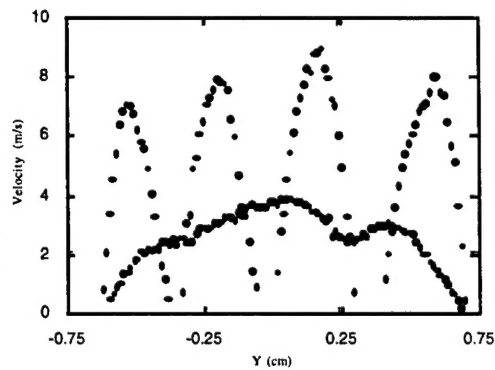
Figure 4. *Top: Photomicrograph of microjet array; bottom left: Schlieren visualization of an operating 4x4 array; bottom right: velocity profiles of near-field emerging jets (4 distinct peaks) and far field merged jet.*

3.3 Accomplishments

3.3.1 Drive Element

Previous microjet devices have been driven with an external piezoelectric element operating at 1.3 kHz. The disadvantages of such devices included relatively high operating voltages (up to 42Vrms) and the unpleasant audible noise due to operation. A new electromagnetic driving element is now being used for microjet research. This new drive element produces jets comparable to those generated by the piezoelectric element yet it operates at lower voltages ($8\text{-}10V_{pp}$) with low power dissipation (up to 300mW). Moreover, the electromagnetic driver operates at a lower frequency range, 150-200Hz, generating considerably less audible noise than previously reported microjet devices.

3.3.2 Modulator Fabrication

Both electrostatic and bimetallic (thermal) actuators as modulators are under consideration. The fabrication sequence for the bimetallic modulators is as follows. Starting with an oxidized <100> silicon substrate, standard photolithography is used to transfer the orifice pattern into the oxide layer on the front side of the wafer. In the second photolithography step, infrared alignment is used to align the same pattern to the oxide layer on the back side of the layer. A sacrificial layer material, such as photoresist or aluminum, is then deposited on the front side of the wafer and patterned using conventional

photolithography. An electroplating seed layer is sputtered over the front surface of the wafer. Copper is electroplated into a patterned plating mold to the desired thickness. Nickel/iron is then electroplated on top of the copper using the same mold. The structure release sequence begins with removal of the electroplating mold and exposed seed layer. The sacrificial material is then etched to release the structure prior to submerging the wafer into a heated potassium hydroxide solution that etches the orifice holes through the wafer.

Significant progress towards fabrication of a complete valve-based microjet device has been made. Theoretical flap deflection models have been constructed for flaps of various dimensions and material compositions. Shown in Figure 3 are photographs of fabricated devices. Figure 3a shows a variety of bimetallic structures fabricated on a glass substrate for deflection testing. Figure 3b shows a photograph of a fabricated 2x2 microjet array prior to driver attachment. The orifices are located in the top center of the photograph under the tips of the cantilever beam modulators.
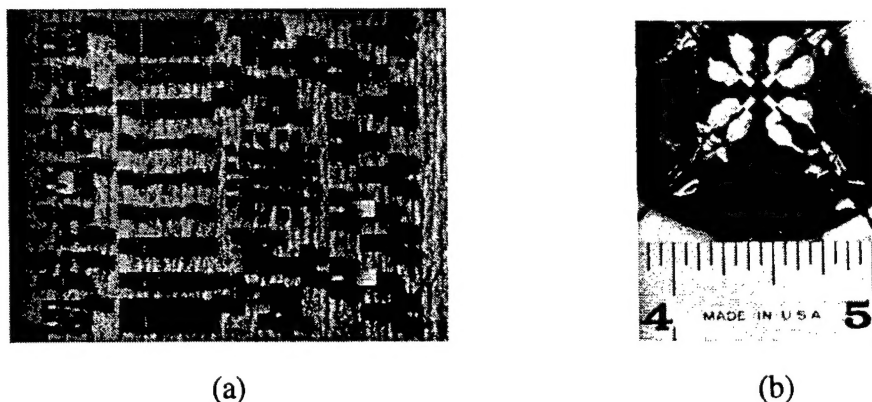

(a)   (b)

Figure 5. Fabricated modulators and microjets. (a) Photograph of fabricated bimetallic flap test structures on glass substrate; (b) Photograph of fabricated 2x2 valve-based microjet array prior to attachment of external membrane and driver. An orifice is located under the tip of each micromachined beam. Test leads are also visible in this photograph. Ruler scale is in inches.

In addition to the silicon-based microjet actuators, the concept of robust devices initiated in this grant has been expanded and leveraged using other contracts to expand the materials base. An example of this is given for electronic cooling applications below.

An example of this approach to fabricate large-area microjets intended for electronic cooling applications is given below. The actuator consists of a corrugated parylene membrane carrying a stencil-printed permanent magnet, and is approximately 1 cm in diameter. A planar coil for electromagnetic actuation is fabricated on the other side of the substrate. A commercially available printed circuit board with a single copper layer is used as substrate material. In a first step, 1 cm recess holes defining the final membrane sizes are drilled into the laminated epoxy board from the backside (Figure 6 (top left)). Additional 1 mm holes are drilled through the substrate in the membrane center to allow the final sacrificial layer etch. A copper foil is laminated onto the backside of the epoxy substrate in a press with a force and temperature of 3.125 tons and 100 °C, respectively. The lamination process forms circular copper membranes with a diameter of 1 cm suspended over the recess holes. A corrugation profile and a flat zone in the membrane center are then etched into the copper layer. The 14 circular corrugations have a height of 80 μm and a period of 200 μm. Then, a 2 μm parylene film is deposited by plasma coating on top of the corrugated copper membranes. Polymer permanent magnets [5] with a diameter of 4 mm, and a thickness of 1 mm are stencil-printed onto the flat zone in the

membrane center. After curing and remagnetizing the magnet, the copper in the area of the diaphragms is etched through the 1 mm holes in a ferric chloride solution. A photograph of the corrugated parylene membrane with the stencil-printed polymer magnet is shown in Figure 6 (bottom). Once the parylene diaphragms are released, the planar coils are fabricated on the opposite side of the substrate using standard photolithography (Figure 6 (top right)). The planar, square coil consists of 31 turns with a wire thickness of 15 μm, and a width and spacing of 40 μm. The planar coils have a typical resistance of 20 to 30 Ω. Instead of a stencil-printed polymer magnet, a commercially available Nd-Fe-B magnet can be mounted in an hybrid fashion onto the parylene diaphragms. Both types of magnetic microactuators have been fabricated.

The fabricated actuators have maximum deflections of 60 μm at 100 mA for NdFeB magnets, and 35 μm at 300 mA for the polymer magnet have been achieved. Under AC excitation, the actuators are audible in the range from 1 to 3 kHz, and produce the strongest synthetic jets in the 50-100 Hz range. It is anticipated that even though the AASERT funding is now ended, this development of robust microjet actuators will continue.
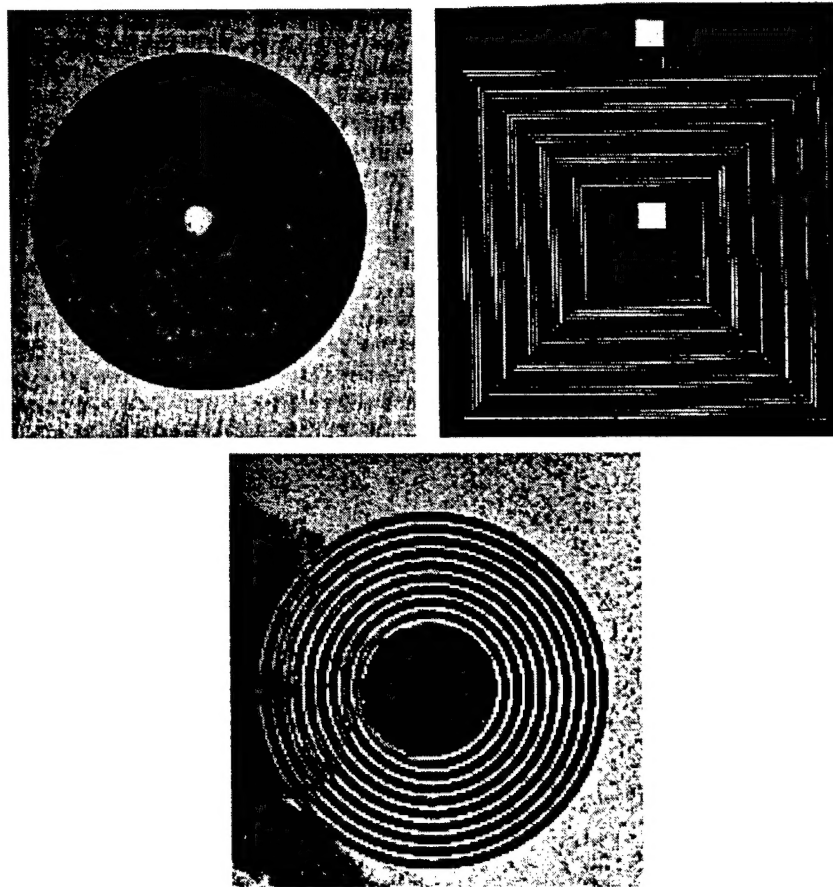

Figure 6 *Large area microjet during various stages of fabrication*

4. Publications

1. Wills, D. S., Lacy, W. S., Camperi-Ginestet, C., Buchanan, B., Jokerst, N. M., Brooke, M. A., "A Fine-Grain, High-Throughput Architecture Using Through-Wafer Optical Communication," *IEEE Journal of Lightwave Technology*, Vol. 13, No. 4, pp. 1085-1092, June, 1995.

2. N. M. Jokerst, C. Camperi-Ginestet, B. Buchanan, S. Wilkinson, M. Brooke, "Communication Through Stacked Silicon Circuitry Using Integrated Thin Film InP-Based Emitters and Detectors," *IEEE Photonics Technology Letters*, Vol. 7, No. 9, pp. 1028-1030, September, 1995.

3. N. Jokerst, M. Brooke, O. Vendier, S. Wilkinson, S. Fike, M. Lee, E. Twyford, J. Cross, B. Buchanan, S. Wills, "Thin Film Multimaterial Optoelectronic Integrated Circuits," *IEEE Transactions on Components, Packaging, and Manufacturing Technology, Part B*, Vol. 19, No. 1, February, 1996, Invited.

4. Coe, D.J.; Allen, M.G.; Smith, B.L.; Glezer, A. "Addressable micromachined jet arrays", 8th International Conference on Solid-State Sensors and Actuators and Eurosensors IX . Digest of Technical Papers, p.329-32 vol.2, 1995

5. Lagorce, L., and Allen, M.G., "Micromachined Polymer Magnets", 1996 IEEE Microelectromechanical Systems Meeting, Technical Digest, San Diego, CA, February, 1996

6. Coe, D.J.; Allen, M.G.; Smith, B.L.; Glezer, A. "Micromachined Jets for Manipulation of Macro Flows", 1994 Solid State Sensors and Actuators Conference, Hilton Head, SC, 1994